Desalination and Water Treatment
www.deswater.com
doi: 10.1080/19443994.2014.986205

57 (2016) 2081–2088
January

Taylor & Francis
Taylor & Francis Group

Synthesis and characterization of $YVO_4:Eu^{3+}$ nanoparticles: kinetics and isotherm studies for the removal of Cd^{2+} metal ion

Mu. Naushad[a], Anees A. Ansari[b,*], Zeid A. ALOthman[a], Jyoti Mittal[c]

[a]*Department of Chemistry, College of Science, Bld#5, King Saud University, Riyadh, Saudi Arabia*
[b]*King Abdullah Institute for Nanotechnology, King Saud University, Riyadh, Saudi Arabia, email: aneesaansari@gmail.com*
[c]*Department of Chemistry, Maulana Azad National Institute of Technology, Bhopal, India*

Received 29 March 2014; Accepted 17 October 2014

ABSTRACT

The prepared $YVO_4:Eu^{3+}$ nanoparticle was successfully used for the removal of highly toxic Cd^{2+} metal ion. Batch experiments were performed as a function of various experimental parameters such as effect of pH (2–8), contact time (5–120 min), initial Cd^{2+} concentration (25–200 mg L^{-1}), and temperature (25–40 °C). The equilibrium was established within 90 min where 82% Cd^{2+} was adsorbed using $YVO_4:Eu^{3+}$ nanoparticles. Kinetic studies showed better applicability for pseudo-second-order model. Langmuir and Freundlich isotherm models were employed for fitting the equilibrium data, and it was found that the Langmuir model fitted the data better than the Freundlich model.

Keywords: $YVO_4:Eu^{3+}$ nanoparticles; Adsorption; Toxic metal; Langmuir adsorption isotherm

1. Introduction

Heavy metal ions such as lead, nickel, copper, zinc, mercury, arsenic, chromium, and cadmium have a significant impact on our aqueous environments. Contamination of aquatic media by these heavy metals is a serious environmental problem, mainly entered into water bodies in the form of effluents from various industries [1–6]. Heavy metals are poisonous contaminants which can accumulate in living tissues causing various disorders and diseases. Cadmium is one of the most toxic metal ions because cadmium tends to accumulate in the kidneys and is associated with renal damage [7], lower bone mineral density, and increase risk of fractures [8]. The removal of heavy metals has always been a major environmental issue. Therefore, how to treat wastewater and make them reusable is not only an important task, but also a serious problem to be solved. The most widely used methods for the removal of heavy metals from wastewaters are chemical precipitation, coagulation, ion exchange, adsorption, solvent extraction, reverse osmosis, electrolysis, and membrane filtration [9]. However, these techniques have certain disadvantages such as operational cost, incomplete removal, high energy requirement, and generation of toxic sludge or other waste products that again require disposal. But, adsorption is one of the most attractive and effective techniques due to its high efficiency, low cost, and easy design [10–14]. Several types of nanoparticles have been used for the removal of Cd^{2+} metal ions from aqueous medium [15,16]. But, to the best of our knowledge, nobody used $YVO_4:Eu^{3+}$ nanoparticles for the removal of Cd^{2+} metal ion. In this study, $YVO_4:Eu^{3+}$ nanoparticles were found to be selective for Cd^{2+} metal ion. The physicochemical properties of $YVO_4:Eu^{3+}$ nanoparticles were

*Corresponding author.

determined using some instrumental analyses viz X-ray diffraction (XRD), field emission transmission electron microscope (FETEM), and UV–visible spectrophotometer. The effects of several operating parameters such as contact time, pH, initial Cd^{2+} ion concentration, and temperature were investigated to achieve the optimum conditions for the adsorption of Cd^{2+} metal ions using YVO_4:Eu^{3+} nanoparticles. Various kinetic models as well as isotherm models have been studied for their usefulness in correlating the experimental data.

2. Experimental

2.1. Reagents and instruments

Yttrium oxide (99%, BDH, England), europium oxide (99.99%, Alfa Aesar, Germany), NH_4VO_3 (Alfa Aesar, USA), citric acid (E Merck Germany), NaOH, HNO_3, and NH_4OH were used as starting materials without any further purification. $Y(NO_3)_3{\cdot}6H_2O$ and $Eu(NO_3)_3{\cdot}6H_2O$ were prepared by dissolving the corresponding oxides in dilute nitric acid. All other reagents and chemicals were of analytical reagent grade. The standard stock solutions of Cd^{2+} metal ion were prepared by dissolving appropriate amounts of cadmium nitrate salts in demineralized water (DMW).

The XRD of the powder samples was examined at room temperature with the use of PANalytical X'Pert X-ray diffractometer equipped with a Ni filtered using Cu K_α ($\lambda = 1.54056$ Å) radiations as X-ray source. The size and morphology of the samples were inspected using a FETEM (JEM-2100F, JEOL, Japan) by operating at an accelerating voltage of 200 kV. The UV/vis absorption spectra were measured a PerkinElmer Lambda-40 spectrophotometer, with the sample contained in 1-cm^3 stoppered quartz cell of 1-cm path length, in the range of 190–600 nm. Single electrode pH meter (Orion 2 star, Thermo Scientific, USA) was used for the pH study. The concentration of Cd^{2+} metal ion was determined by atomic absorption spectrometer (AAS, PerkinElmer, USA). All measurements were performed at room temperature.

2.2. Synthesis of luminescent YVO_4:Eu^{3+} nanoparticles

In a typical synthesis, NaOH (120 mg), citric acid (0.5 g), and NH_4VO_3 (0.1 mmol) were dissolved into 50 mL of deionized water under stirring. Then, an aqueous solution of $Y(NO_3)_3{\cdot}6H_2O$ and $Eu(NO_3)_3{\cdot}6H_2O$ (1 mmol total, of which 5 mmol% was of the luminescent ion) in 10 mL DMW was slowly added into the mixture solution, and stirring was maintained at 80°C for another 3 h. Subsequently, aqueous ammonia (NH_4OH) solution was added drop wise into the solution and the pH value was carefully adjusted to 8–9 [17]. After naturally cooling to room temperature, the resultant solid products were centrifugally separated from the suspension, washed with DMW and absolute ethanol several times, and dried at 60°C in air for 6 h.

2.3. Batch adsorption studies

The adsorption of Cd^{2+} onto YVO_4:Eu^{3+} nanoparticles were carried out by batch method. The adsorption experiments were carried out in 100-mL glass conical flasks covered with Teflon sheets to prevent the introduction of any foreign particle contamination. A fixed amount of YVO_4:Eu^{3+} nanoparticles (30 mg) was added to 50 mL of Cd^{2+} solution of known concentration in conical flask which was placed in thermostat-cum-shaking assembly. The solution was stirred continuously at constant temperature for 2 h to achieve the equilibration time. After equilibration time, the solid part was filtered off using Whatman filter No. 41 and equilibrium concentration of Cd^{2+} was determined by AAS. A number of parameters such as contact time, pH, initial concentration of Cd^{2+}, and temperature were changed in order to optimize the adsorption process.

The amount of Cd^{2+} per unit weight of adsorbent, q_e (mg g^{-1}), was calculated by the following equation:

$$q_e = \frac{V(C_o - C_e)}{W \times 1,000} \quad (1)$$

where V is the volume of Cd^{2+} solution in liter, C_o and C_e are the initial and final concentrations (mg L^{-1}) of Cd^{2+} in solution, respectively, W is the weight (g) of YVO_4:Eu^{3+} nanoparticles.

Kinetics studies were performed by varying the Cd^{2+} ion initial concentration (C_o, 25–75 mg L^{-1}). The samples were collected at specified time intervals until equilibrium attained. Isotherm studies were performed by varying the reaction temperature (25–40°C) and initial concentration of Cd^{2+} solution (25–200 mg L^{-1}).

3. Results and discussion

3.1. Characterization

The YVO_4:Eu^{3+} nanoparticles were characterized by XRD, FETEM, and UV–visible spectrophotometer. Wide-angle XRD pattern was utilized to investigate the crystalline nature and phase purity of the synthesized product. The XRD pattern exhibited all characteristic

diffraction peaks of pure crystalline tetragonal zircon-type structure YVO_4 with a space group of I_{41}/amd. The peak positions and intensities were in accord with the literature values for the pure tetragonal phase of the corresponding bulk materials (JCPDS No. 17-0341) [17–19]. No trace of impurity peaks was observed within the detection limit of our XRD, which indicated the phase purity of the synthesized nanoparticles (Fig. 1). Average crystallite size of 5% Eu^{3+}-doped YVO_4 nanoparticles was found to be 30 nm, as estimated using the Debye–Scherer equation:

$$D = (\alpha\lambda)/(\beta\cos\theta) \quad (2)$$

where D is the mean particle size, λ is X-ray wavelength (1.541 Å), θ is the Bragg angle, and β is half-width at full maxima of diffraction peak.

FETEM micrographs were used to examine the morphology and size of the synthesized YVO_4:Eu^{3+} nanoparticles as shown in Fig. 2. The micrograph showed that the prepared nanocrystals were irregular in shape and size and were highly aggregated with a narrow size distribution. The TEM image is given in Fig. 2(inset) displayed the lattice fringes for nanoparticles, indicated that these YVO_4:Eu^{3+} nanoparticles possessed high crystallinity. The calculated interplanar distance between the adjacent lattice fringes was in good agreement with the (200) spacing of the standard value (0.352 nm) and lattice planes of tetragonal YVO_4 (JCPDS No. 17-0341), which further confirmed that the high-crystallinity and single crystal feature of as-prepared sample [19]. UV/vis spectrum of YVO_4:Eu^{3+} nanoparticles showed a broad absorption band located at 290 nm, charge-transfer absorption from the oxygen to the central vanadium atoms inside the VO_4, which agreed with the spectra of previous observations (Fig. 3) [12]. The absorption was caused by a charge-transfer transition from the oxygen ligands to the central vanadium atom inside the VO_4^{3-} ion, and the energy was subsequently transferred to the Eu^{3+} ion, as expected. This absorption peak could be assigned to $^1A_1 \rightarrow {}^1T_1$ ($t_1 \rightarrow 2e$) transition of the VO_4^{3-} ion. Generally, the $^1A_1 \rightarrow {}^1T_1$ ($t_1 \rightarrow 2e$) transition is forbidden, as the size of the particles decreases and the deformation of the structure increases, $^1A_1 \rightarrow {}^1T_1$ transition could be partly allowed [20].

The adsorption of Cd^{2+} onto YVO_4:Eu^{3+} nanoparticles was carried out at different time interval (5–120 min). It is apparent from Fig. 4(a) that the adsorption was fast at the initial stages and equilibrium was attained at 90 min where 82% Cd^{2+} metal was adsorbed. The difference in the rate of adsorption may be due to the fact that initially, all adsorbent sites were vacant so the adsorption was high. Later, due to the decrease in number of adsorption sites as well as Cd^{2+} concentration, the Cd^{2+} uptake rate by YVO_4:Eu^{3+} nanoparticles became slow [21]. The effect of pH for the adsorption of Cd^{2+} onto YVO_4:Eu^{3+} nanoparticles was testified in the pH range 2–8. The optimum pH for the maximum removal of Cd^{2+} was found to be 7 (Fig. 4(b)). After pH 7, the adsorption became constant because at pH > 7.0, the Cd^{2+} gets precipitated due to the hydroxide anions formed cadmium hydroxide precipitate. The effect of temperature on the adsorption of Cd^{2+} metal ion was studied by varying the temperature from 25 to 40°C at pH 7 for 90 min (Fig. 4(c)). It was observed that the adsorption of Cd^{2+} was increased from 47.8 to 84% as the temperature was increased 25–40°C which demonstrated the endothermic nature of Cd^{2+} adsorption onto YVO_4:Eu^{3+} nanoparticles. The adsorption of Cd^{2+} metal onto YVO_4:Eu^{3+} nanoparticles was also studied by varying

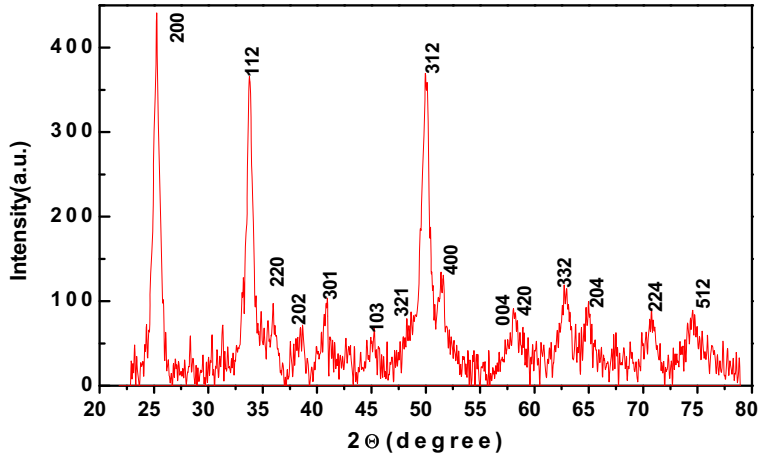

Fig. 1. XRD pattern of the YVO_4:Eu^{3+} nanoparticles.

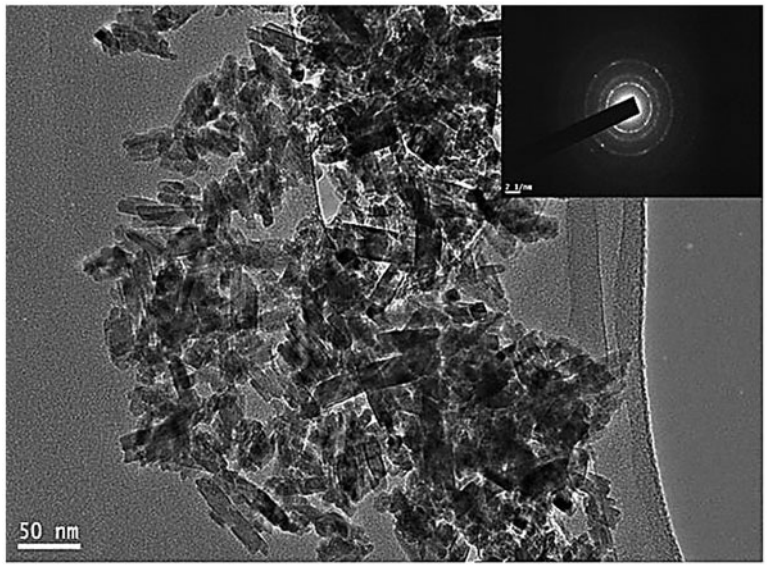

Fig. 2. FE-TEM image of the YVO_4:Eu^{3+} nanoparticles and inset shows selected area electron diffraction.

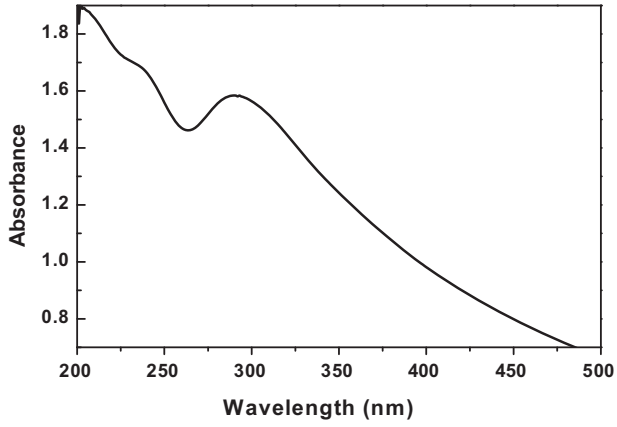

Fig. 3. UV/vis absorption spectrum of the YVO_4:Eu^{3+} nanoparticles in ethanol.

initial cadmium concentration (25–200 mg L^{-1}) (Fig. 4(d)). It was found that the percentage removal of Pb^{2+} was decreased from 83 to 62% as the concentration of Cd^{2+} was increased from 25 to 200 mg L^{-1} which may be due to the less availability of adsorption sites at higher dose of Cd^{2+}.

3.2. Adsorption kinetics

3.2.1. The pseudo-first-order equation

The rate constant k_1 for the adsorption of Cd^{2+} was studied by Lagergren rate equation for initial Cd^{2+} concentration of 25, 50, and 75 mg L^{-1} [22].

$$\log(q_e - q_t) = \log q_e - \frac{k_1 t}{2.303} \quad (3)$$

where q_t and q_e are the amounts of Cd^{2+} adsorbed at time t and at equilibrium, respectively, and k_1 is the rate constant for pseudo-first-order adsorption (min^{-1}). The values of rate constant were determined from the slope of the plot log ($q_e - q_t$) vs. t.

3.2.2. The pseudo-second-order equation

The pseudo-second-order kinetic rate equation was given by Ho and McKay [23]:

$$\frac{t}{q_t} = \frac{1}{k_2 {q_e}^2} + \frac{t}{q_e} \quad (4)$$

where k_2 is the pseudo-second-order rate constant. The values of k_2 for all studied concentrations were determined from the intercepts of the plot t/q_t vs. time. Fig. 5((a) and (b)) presents the plots for pseudo-first-order and pseudo-second-order kinetic models, respectively. The parameters obtained for two models are presented in Table 1. It is apparent from Table 1 that the values of correlation coefficients (R^2) for pseudo-second-order model were higher than pseudo-first-order model which indicated that the adsorption system studied belongs to the second-order kinetic model.

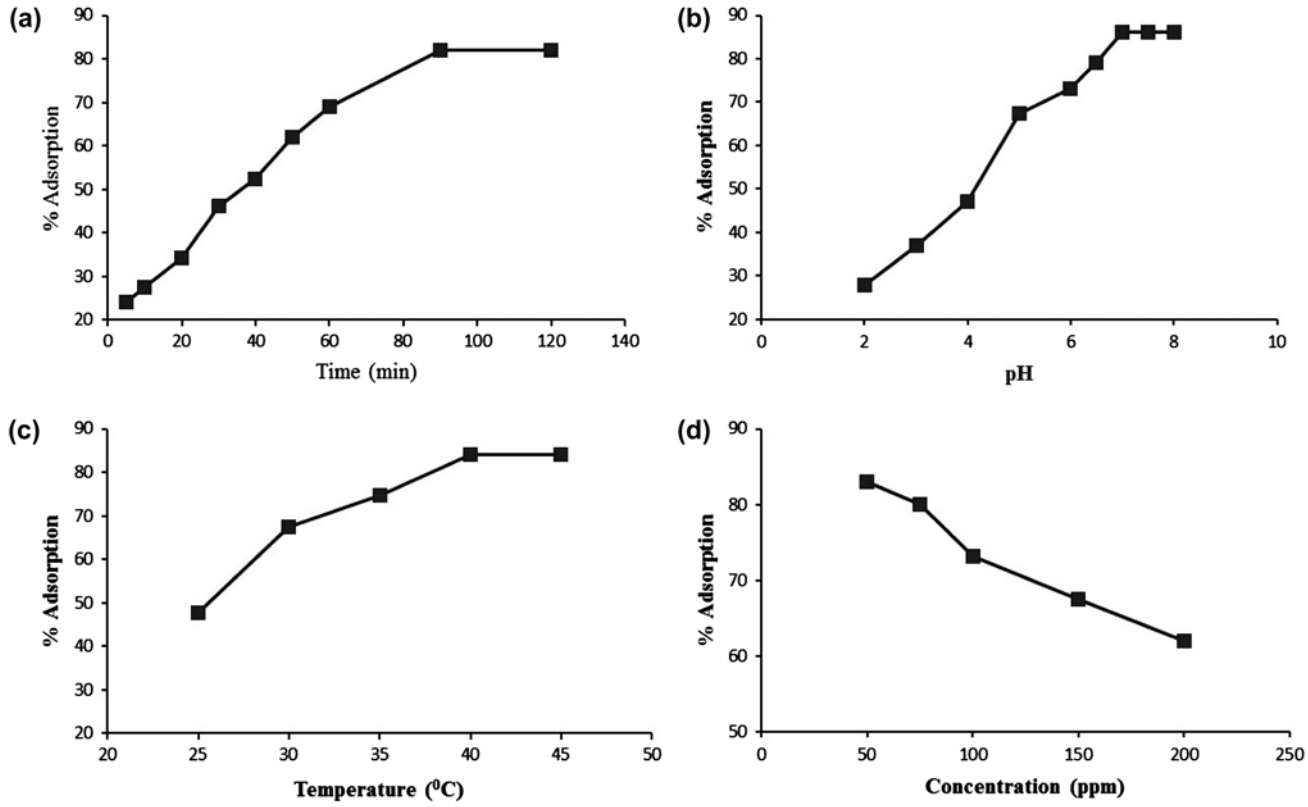

Fig. 4. Percentage removal of Cd^{2+} metal ion using YVO_4:Eu^{3+} nanoparticles at different (a) time, (b) pH, (c) temperature, and (d) initial Cd^{2+} metal ion concentration.

3.3. Adsorption isotherms

3.3.1. Langmuir isotherm model

The Langmuir model assumes that the uptake of adsorbate molecules occurs on a homogenous surface with a finite number of adsorption sites by monolayer adsorption without any interaction between adsorbed molecules. Once a site is occupied by adsorbate molecules, no further adsorption can occur at that site. The surface will reach the saturation point, and the maximum adsorption of the surface will be achieved. The Langmuir isotherm [24] model can be expressed as:

$$\frac{1}{q_e} = \frac{1}{Q_0} + \frac{1}{bQ_0C_e} \tag{5}$$

where q_e is the amount of Cd^{2+} adsorbed (mg g^{-1}), C_e is the equilibrium concentration of Cd^{2+} (mg L^{-1}), Q_0 and b are the Langmuir constants related to maximum monolayer adsorption capacity and energy of adsorption, respectively. The values of Q_0 and b were evaluated from the intercept and slope of linear plots of $1/q_e$ vs. $1/C_e$, respectively (Fig. 6(a) and (b)).

In order to predict the adsorption efficiency of the adsorption process, the dimensionless equilibrium

Table 1
Kinetic constant parameters for the adsorption of Cd^{2+} metal ion using YVO4:Eu^{3+} nanoparticles

	Pseudo-first order				Pseudo-second order			
Initial concentration (mg L^{-1})	Slope	Intercept	k_1 (min^{-1})	R^2	Slope	Intercept	k_2 (g mg^{-1} min^{-1})	R^2
25	−0.0134	1.60	3.08×10^{-2}	0.928	0.0192	0.603	6.11×10^{-4}	0.989
50	−0.0133	1.89	3.06×10^{-2}	0.921	0.0098	0.315	3.04×10^{-4}	0.987
75	−0.0131	2.07	3.01×10^{-2}	0.926	0.0065	0.223	1.9×10^{-4}	0.985

Table 2
Adsorption isotherm constants for the adsorption of Cd^{2+} metal ion using YVO4:Eu^{3+} nanoparticles

Temperature (°C)	Langmuir constants			Freundlich constants			
	Q_o (mg g^{-1})	b (L mg^{-1})	R^2	$1/n$	n	K_f	R^2
25	99.01	8.21×10^{-3}	0.986	0.943	1.06	2.36	0.940
30	149.25	7.83×10^{-3}	0.986	0.935	1.07	3.05	0.940
35	156.25	8.56×10^{-3}	0.988	0.934	1.07	1.76	0.941
40	86.20	17.9×10^{-3}	0.985	0.998	1.03	1.27	0.936

parameter (R_L) known as separation factor was determined using the following equation [25]:

$$R_L = \frac{1}{1 + K_L C_o} \tag{6}$$

where C_o (mg L^{-1}) is the lowest initial concentration of Cd^{2+} and K_L is the Langmuir adsorption constant (L mg^{-1}). The R_L value confirms the adsorption to be unfavorable ($R_L > 1$), linear ($R_L = 1$), favorable ($0 < R_L < 1$), or irreversible ($R_L = 0$). The values of R_L for each initial concentration used were greater than zero and less than unity which indicated the favorable adsorption of Cd^{2+} onto YVO_4:Eu^{3+} nanoparticles.

3.3.2. Freundlich isotherm model

The linearized form of Freundlich isotherm is expressed by the following equation:

$$\log q_e = \log K_f + \frac{1}{n} \log C_e \tag{7}$$

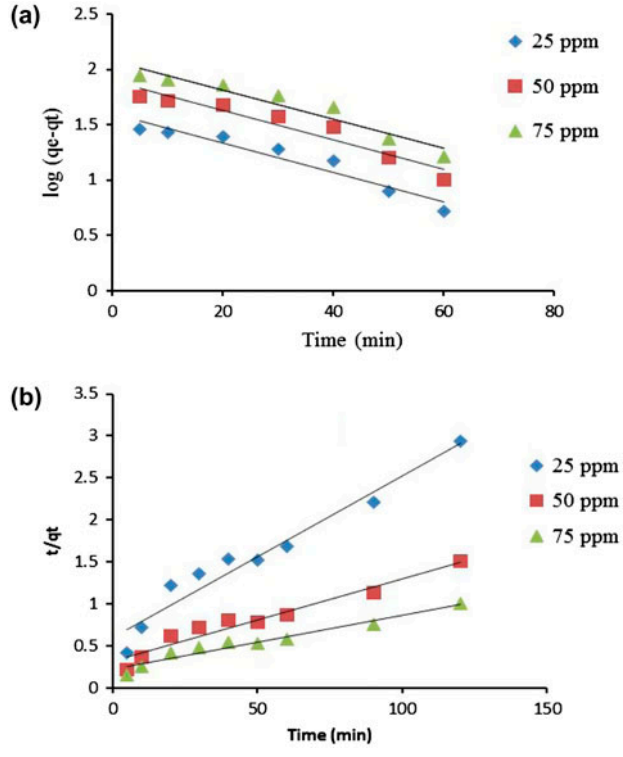

Fig. 5. Kinetic models for the adsorption of Cd^{2+} metal ion using YVO_4:Eu^{3+} nanoparticles (a) pseudo-first-order and (b) pseudo-second-order.

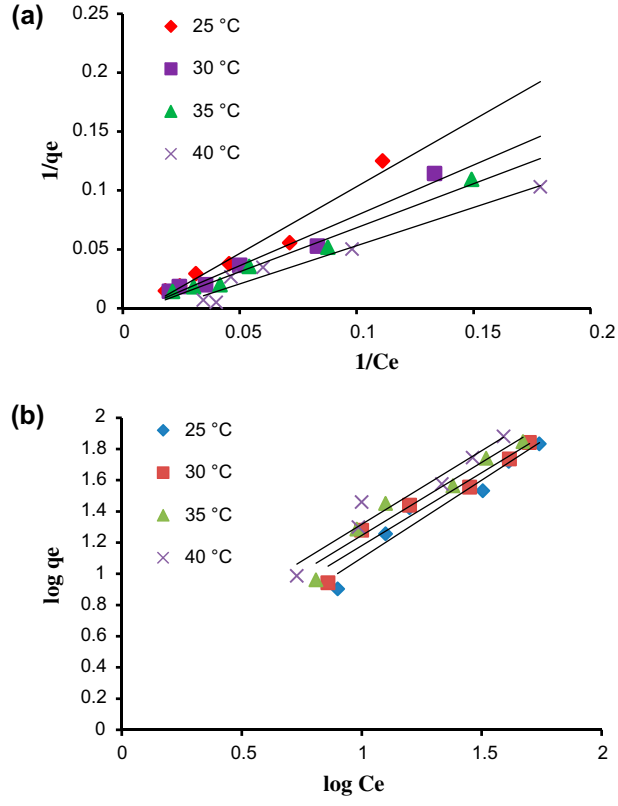

Fig. 6. Adsorption isotherm models for the adsorption of Cd^{2+} metal ion using YVO_4:Eu^{3+} nanoparticles (a) Langmuir and (b) Freundlich.

where K_f and n are the Freundlich isotherm constants related to adsorption capacity (mg g^{-1}) and adsorption intensity of YVO_4:Eu^{3+} nanoparticles, respectively. The values of n and K_f were obtained from the slope $(1/n)$ and intercept (log K_f) of the plot of log q_e vs. log C_e, respectively. The value of n is an indication of the favorability of adsorption. Values of $n > 1$ represent favorable nature of adsorption. The value of $n > 1$ for Cd^{2+} indicated the favorable adsorption by YVO_4:Eu^{3+} nanoparticles at different concentrations. The parameters derived by fitting these two isotherm models are presented in Table 2. The Langmuir model showed the better correlation coefficient values ($R^2 > 0.985$) which indicated the better applicability of Langmuir model.

4. Conclusion

In this study, YVO_4:Eu^{3+} nanoparticles were synthesized and used for the removal of highly toxic Cd^{2+} metal ion. The highest adsorption of Cd^{2+} metal ion was observed at pH 7 and 40°C. The kinetics data were best fitted in pseudo-second-order rate equation as apparent from the values of regression coefficients. The adsorption isotherm studies showed that Langmuir model was the best fit model.

Acknowledgment

This project was supported by King Saud University, Deanship of Scientific Research, College of Science Research Center.

References

[1] M. Monier, D.M. Ayad, Y. Wei, A.A. Sarhan, Adsorption of Cu(II), Co(II), and Ni(II) ions by modified magnetic chitosan chelating resin, J. Hazard. Mater. 177 (2010) 962–970.
[2] N. Kuyucak, Acid mine drainage prevention and control options, CIM Bull. 95 (1999) 96–102.
[3] L.H. Filipek, C. Hatton, J. Gusek, T. Tsukamoto, Passive treatment of acid rock drainage (ARD): State of the practice, in: Proceedings of the Tenth International Conference on Tailings and Mine Waste, October, Colorado, USA, 2003, pp. 293–303.
[4] S.A. Nabi, Mu. Naushad, Studies of cation-exchange thermodynamics for alkaline earths and transition metal ions on a new crystalline cation-exchanger aluminium tungstate: Effect of the surfactant's concentration on distribution coefficients of metal ions, Colloids Surf., A 293 (2007) 175–184.
[5] S.A. Nabi, Mu. Naushad, A new electron exchange material Ti(IV) iodovanadate: Synthesis, characterization and analytical applications, Chem. Eng. J. 158 (2010) 100–107.
[6] S.A. Nabi, S.A. Ganai, Mu. Naushad, A new Pb(II) ion selective hybrid cation exchanger EDTA–Zirconium iodate: Synthesis, characterization and analytical applications, Ads. Sci. Tech. 26 (2009) 463–478.
[7] L. Jarup, M. Berglund, C.G. Elinder, G. Nordberg, M. Vahter, Health effects of cadmium exposure—A review of the literature and a risk estimate, Scand. J. Work Environ. Health 24 (1998) 1–52.
[8] L. Järup, T. Alfvén, Low level cadmium exposure, renal and bone effects—The OSCAR study, BioMetals 17 (2004) 505–509.
[9] J.W. Moore, Inorganic Contaminants of Surface Water Residuals and Monitoring Priorities, Springer, New York, NY, 1994, pp. 178–210.
[10] M. Naushad, Surfactant assisted nano-composite cation exchanger: Development, characterization and applications for the removal of toxic Pb^{2+} from aqueous medium, Chem. Eng. J. 235 (2014) 100–108.
[11] Mu Naushad, Removal of malathion from aqueous solution using De-Acidite FF-IP resin and determination by UPLC–MS/MS: Equilibrium, kinetics and thermodynamics studies, Talanta 115 (2013) 15–23.
[12] Mu. Naushad, Z.A. ALOthman, M.R. Khan, S.M. Wabaidur, Removal of bromate from water using de-acidite FF-IP resin and determination by ultra-performance liquid chromatography–tandem mass spectrometry, Clean Soil Air Water 41 (2013) 528–533.
[13] Z.A. AlOthman, M.M. Alam, Mu. Naushad, Heavy toxic metal ion exchange kinetics: Validation of ion exchange process on composite cation exchanger nylon 6,6 Zr(IV) phosphate, J. Ind. Eng. Chem. 19 (2013) 956–960.
[14] Mu. Naushad, M.R. Khan, S.M. Wabaidur, A comparative study on characterization of aluminium tungstate and surfactant based aluminium tungstate cation exchangers: Analytical applications for the separation of toxic metal ions, J. Inorg. Organomet. Polym. 22 (2011) 352–359.
[15] L. Zhu, L. Xu, B. Huang, N. Jia, L. Tan, S. Yao, Simultaneous determination of Cd(II) and Pb(II) using square wave anodic stripping voltammetry at a gold nanoparticle-graphene-cysteine composite modified bismuth film electrode, Electrochim. Acta. 115 (2014) 471–477.
[16] Y. Gao, R. Wahi, A.T. Kan, J.C. Falkner, V.L. Colvin, M.B. Tomson, Adsorption of cadmium on anatase nanoparticles—Effect of crystal size and pH, Langmuir 20 (2004) 9585–9593.
[17] A.A. Ansari, M. Alam, J. Labis, S.A. Alrokayan, G. Shafi, T.N. Hasan, N.A. Syed, A. Alshatwi, Luminescent mesoporous $LaVO_4$:Eu^{3+} core-shell nanoparticles: Synthesis, characterization, biocompatibility and their cytotoxicity, J. Mater. Chem. 21 (2011) 19310–19317.
[18] A.A. Ansari, J.P. Labis, S.A. Alrokayan, Synthesis of water-soluble luminescent $LaVO_4$:Ln^{3+} porous nanoparticles, J. Nanoparticle Res. 14 (2012) 999.
[19] N.S. Singh, R.S. Ningthoujam, L.R. Devi, N. Yaiphaba, V. Sudarsan, Luminescence study of Eu^{3+} doped $GdVO_4$ nanoparticles: Concentration, particle size, and core/shell effects, J. Appl. Phys. 104 (2008) 104307–104316.

[20] X. Wu, Y. Tao, C. Song, C. Mao, L. Dong, J. Zhu, Morphological control and luminescent properties of YVO_4:Eu nanocrystals, J. Phys. Chem. B 110 (2006) 15791–15796.
[21] M. Naushad, Z.A. ALOthman, M. Islam, Adsorption of cadmium ion using a new composite cation-exchanger polyaniline Sn(IV) silicate: Kinetics, thermodynamic and isotherm studies, Int. J. Environ. Sci. Technol. 10 (2013) 567–578.
[22] S. Lagergren, About the theory of so called adsorption of soluble substances, K. Sven. Vetenskapsakad. Handl. 24 (1898) 1–39.
[23] Y.S. Ho, G. McKay, Sorption of dye from aqueous solution by peat, Chem. Eng. J. 70 (1998) 115–124.
[24] I. Langmuir, The constitution and fundamental properties of solids and liquids. Part I. Solids, J. Am. Chem. Soc. 38 (1916) 2221–2295.
[25] K.R. Hall, L.C. Eagleton, A. Acrivos, T. Vermeulen, Pore-and solid-diffusion kinetics in fixed-bed adsorption under constant-pattern conditions, I&EC Fundam. 5 (1966) 212–223.